AGU PUBLICATIONS

JGR

Journal of Geophysical Research: Space Physics

RESEARCH ARTICLE

10.1002/2016JA022958

Key Points:

- Compressional Pc3 waves were detected in the magnetosphere both on the dayside and nightside with global coherence in amplitude modulation
- Phase delay analysis using three spacecraft in the midnight sector indicates duskward propagation of the waves
- The oscillations are attributed to fast-mode waves originating from ULF waves generated in the ion foreshock

Correspondence to:
K. Takahashi,
kazue.takahashi@jhuapl.edu

Citation:
Takahashi, K., M. D. Hartinger, D. M. Malaspina, C. W. Smith, K. Koga, H. J. Singer, D. Frühauff, D. G. Baishev, A. V. Moiseev, and A. Yoshikawa (2016), Propagation of ULF waves from the upstream region to the midnight sector of the inner magnetosphere, *J. Geophys. Res. Space Physics*, *121*, 8428–8447, doi:10.1002/2016JA022958.

Received 16 MAY 2016
Accepted 17 AUG 2016
Accepted article online 22 AUG 2016
Published online 10 SEP 2016

Propagation of ULF waves from the upstream region to the midnight sector of the inner magnetosphere

Kazue Takahashi[1], Michael D. Hartinger[2], David M. Malaspina[3], Charles W. Smith[4], Kiyokazu Koga[5], Howard J. Singer[6], Dennis Frühauff[7], Dmitry G. Baishev[8], Alexey V. Moiseev[8], and Akimasa Yoshikawa[9,10]

[1]The Johns Hopkins University Applied Physics Laboratory, Laurel, Maryland, USA, [2]Bradley Department of Electrical and Computer Engineering, Virginia Polytechnic Institute and State University, Blacksburg, Virginia, USA, [3]Laboratory for Atmospheric and Space Physics, University of Colorado Boulder, Boulder, Colorado, USA, [4]Department of Physics and Institute for the Study of Earth, Oceans and Space, University of New Hampshire, Durham, New Hampshire, USA, [5]Japan Aerospace Exploration Agency, Tsukuba, Japan, [6]NOAA Space Weather Prediction Center, Boulder, Colorado, USA, [7]Institute for Geophysics and Extraterrestrial Physics, Technical University of Braunschweig, Braunschweig, Germany, [8]Yu. G. Shafer Institute of Cosmophysical Research and Aeronomy (IKFIA) Siberian Branch, Russian Academy of Sciences, Yakutsk, Russia, [9]Department of Earth and Planetary Science, Kyushu University, Fukuoka, Japan, [10]International Center for Space Weather Science and Education, Kyushu University, Fukuoka, Japan

Abstract Ultralow frequency (ULF) waves generated in the ion foreshock are a well-known source of Pc3-Pc4 waves (7–100 mHz) observed in the dayside magnetosphere. We use data acquired on 10 April 2013 by multiple spacecraft to demonstrate that ULF waves of upstream origin can propagate to the midnight sector of the inner magnetosphere. At 1130–1730 UT on the selected day, the two Van Allen Probes spacecraft and the geostationary ETS-VIII satellite detected compressional 20 to 40 mHz magnetic field oscillations between $L \sim 4$ and $L \sim 7$ in the midnight sector, along with other spacecraft located closer to noon. Upstream origin of the oscillations is concluded from the wave frequency that matches a theoretical model, globally coherent amplitude modulation, and duskward propagation that is consistent with expected entry of the upstream wave energy through the dawnside flank under the observed interplanetary magnetic field. The oscillations are attributed to magnetohydrodynamic fast-mode waves based on their propagation velocity of ~300 km/s and the relationship between the electric and magnetic field perturbations. The magnitude of the azimuthal wave number is estimated to be ~30. There is no evidence that the oscillations propagated to the ground in the midnight sector.

1. Introduction

Upstream ultralow frequency (ULF) waves are a well-known source of fast-mode waves observed in the magnetosphere. The waves are generated in the ion foreshock region by an ion beam cyclotron instability [*Fairfield*, 1969]. Once generated, the waves are convected toward the Earth in the superAlfvénic solar wind flow, are transmitted through the bow shock and magnetopause, and propagate into the magnetosphere as magnetohydrodynamic (MHD) fast-mode waves according to MHD theory [*McKenzie*, 1970; *Wolfe and Kaufmann*, 1975], although wave propagation through the boundaries is more complicated when ion cyclotron waves and mirror-mode waves are taken into account [*Narita and Glassmeier*, 2005]. Spacecraft in the dayside magnetosphere routinely detect the fast-mode waves as compressional magnetic field oscillations in the Pc3 band (22–100 mHz) [*Greenstadt et al.*, 1983; *Yumoto et al.*, 1985; *Takahashi et al.*, 1994; *Heilig et al.*, 2007, 2013; *Clausen et al.*, 2009]. The waves are believed to propagate to the ground and produce Pc3 geomagnetic pulsations on the dayside [*Troitskaya et al.*, 1971; *Vellante et al.*, 1996; *Kim et al.*, 1998]. At times the frequency of the compressional waves may become low and falls into the Pc4 band (7–22 mHz) [*Troitskaya et al.*, 1971; *Troitskaya*, 1994]. Evidence of the upstream source mechanism includes the following: (1) dependence of Pc3-Pc4 wave amplitude on the angle between the interplanetary magnetic field (IMF) and the Sun-Earth line, denoted θ_{xB} and referred to as the IMF cone angle [*Bol'shakova and Troitskaya*, 1968], and (2) dependence of Pc3-Pc4 wave frequency on the magnitude of the IMF [*Troitskaya et al.*, 1971]. When the cone angle is small, upstream waves develop in a large volume in front of the bow shock and the resulting fast-mode waves in the magnetosphere become stronger. As for the frequency of the upstream waves, f_{UW}, a theoretical formula has been derived by *Takahashi et al.* [1984] as

$$f_{\mathrm{UW}}(\mathrm{mHz}) = 7.6B_{\mu}(\mathrm{nT})\cos^2\theta_{xB}, \tag{1}$$

where B_{μ} is the magnetic field magnitude. Equation (1) is close to empirical formulas obtained from ground observations [*Troitskaya and Bolshakova*, 1988] and is in good agreement with spacecraft observations [e.g., *Clausen et al.*, 2009].

A remaining question on fast-mode waves of upstream origin is whether they propagate to the nightside. Previous studies using ground-based experiments provided possible evidence of the propagation. *Takahashi et al.* [2005] suggested that 5 to 20 mHz magnetic pulsations observed on the nightside originated from upstream waves. *Ponomarenko et al.* [2010] presented magnetometer and HF radar observations in support of the propagation. This paper presents the first evidence of the day-to-night propagation in spacecraft data. The waves had perturbations in the magnetic field magnitude mostly in the Pc3 band with a center frequency of ~30 mHz. Accordingly, we term them compressional Pc3 waves.

The remainder of the paper is organized as follows. Section 2 describes experiments and data. Section 3 presents an overview of the observations on 10 April 2013. Section 4 presents analyses of the properties of the waves. Section 5 presents discussion, and section 6 concludes the study.

2. Experiments

We use data from Earth-orbiting spacecraft and ground magnetometers. We have analyzed data from four spacecraft in low-inclination elliptical orbits: Time History of Events and Macroscale Interactions during Substorms (THEMIS) C (also known as ARTEMIS P2), THEMIS D, Radiation Belt Storm Probes (RBSP, also known as Van Allen Probes) A, and RBSP B; and two spacecraft in geostationary orbits: Geostationary Operational Environmental Satellite (GOES-15) (135° west geographic longitude) and Engineering Test Satellite (ETS)-VIII (146° east). The primary data used in the study, magnetic field vectors, were acquired at each of these spacecraft with a three-axis fluxgate magnetometer as described by *Auster et al.* [2008] for THEMIS, by *Singer et al.* [1996] for GOES, by *Koga and Obara* [2008] for ETS-VIII, and by *Kletzing et al.* [2013] for RBSP. Note that we have made an offset correction to the ETS-VIII data following *Nosé et al.* [2014]. We also use electric field data [*Wygant et al.*, 2013] and electron density data (inferred from plasma wave spectra) [*Kurth et al.*, 2015] that are available from the RBSP spacecraft. Electron density can also be inferred from the spacecraft potential measured at RBSP and THEMIS. For observations in the magnetosphere we specify the spacecraft magnetic coordinates using a centered dipole: field line equatorial distance L normalized to Earth radius R_{E} (= 6371.2 km), magnetic latitude (MLAT, in degrees) and magnetic local time (MLT, in hours). The ground magnetometer data have been acquired at Boulder [*Love et al.*, 2015], Pine Ridge [*Russell et al.*, 2008], Bennington [*Chi et al.*, 2013], Zyryanka [*Yumoto and The 210° MM Magnetic Observation Group*, 1996], and Kakioka [*Tsunomura et al.*, 1994].

3. Overview of the Observations

The compressional Pc3 waves featured in this paper were observed on 10 April 2013. We have chosen the time interval 1130–1730 UT for detailed analysis because of a continuous wave activity and good distribution of spacecraft in local time. This section presents an overview of the observations.

Figure 1 illustrates spacecraft positions, IMF parameters, and the dynamic spectra of the magnetic field magnitude (denoted B_{μ}) for the selected 6 h interval. Figure 1a indicates that THEMIS D was located in the prenoon sector, GOES-15 was located in the dawn sector, and RBSP A, RBSP B, and ETS-VIII were located on the nightside. This figure includes the model magnetopause by *Shue et al.* [1998] plotted for solar wind dynamic pressure of 1.3 nPa and IMF B_z of 0.5 nT, which are the averages of 1130–1730 UT, and the model bow shock by *Fairfield* [1971].

THEMIS C was located in the solar wind ~60 R_{E} upstream of the Earth, within 3.5 R_{E} of the Sun-Earth line. Figures 1b–1d show the IMF magnitude, cone angle, and azimuthal angle $\phi_{xy} (\equiv \tan^{-1}(B_y/B_x))$ at THEMIS C, where the field components are given in the Geocentric Solar Ecliptic (GSE) coordinates. The solar wind velocity measured by THEMIS C [*McFadden et al.*, 2008] (data not shown) was nearly constant with an average value of 343 km/s and a standard deviation of 11 km/s, implying that the solar wind took ~15 min to reach the bow

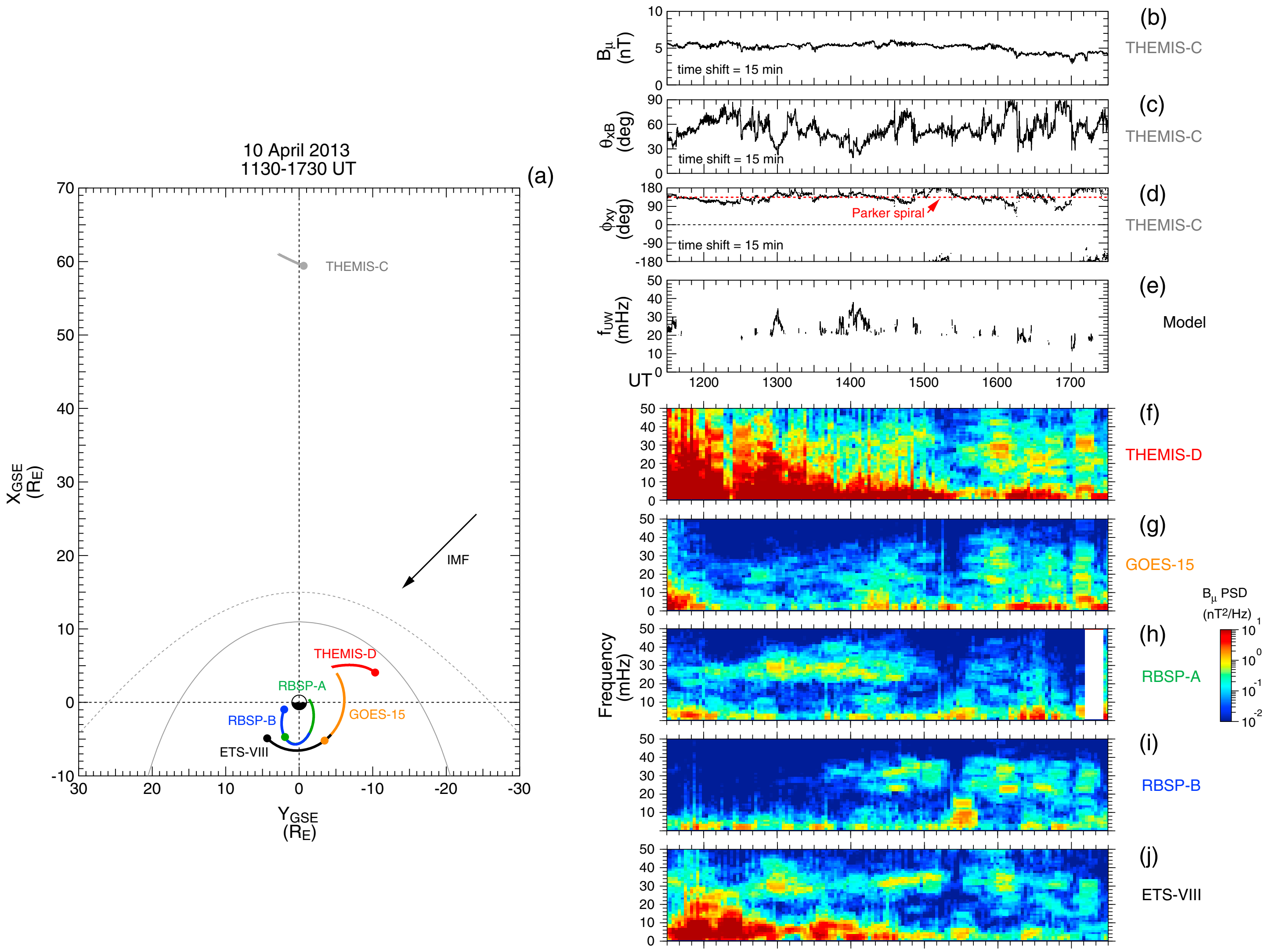

UT	1200	1300	1400	1500	1600	1700	
MLT	7.52	7.74	7.99	8.29	8.66	9.12	THEMIS-D
MLT	2.87	3.87	4.88	5.90	6.94	7.98	GOES-15
MLT	22.93	23.64	0.32	1.09	2.13	4.13	RBSP-A
MLT	20.75	22.11	22.97	23.69	0.39	1.19	RBSP-B
MLT	21.63	22.63	23.65	0.67	1.71	2.75	ETS-VIII

Figure 1. Overview of multispacecraft observations of ULF waves during a 6 h interval on 10 April 2013. (a) Spacecraft positions projected onto the GSE *X-Y* plane. The dots indicate the start positions. The black arrow indicates the IMF direction representative of the time interval shown. (b–d) IMF magnitude B_μ, cone angle θ_{xB}, and azimuthal angle ϕ_{xy} at THEMIS C that are time shifted by 15 min to account for solar wind convection from the spacecraft to the bow shock nose. The red dashed line in the ϕ_{xy} plot indicates a nominal Parker spiral angle of 135°. (e) Upstream wave frequency estimated using the IMF data from THEMIS C, plotted for $\theta_{xB} < 45°$. (f–j) Dynamic spectra of the B_μ component at five spacecraft located in the magnetosphere. The local time of each spacecraft is shown at the bottom.

shock nose from the position of THEMIS C. Accordingly, we have shifted the IMF data by 15 min. The IMF cone angle varied significantly but did not reach very small values which would have generated ULF waves in a large volume in front of the bow shock. The IMF azimuthal angle was mostly in the 90–180° range with an average close to the nominal Parker spiral angle of 135°, shown by a red dashed line in Figure 1d. With this IMF orientation (see the black arrow in Figure 1a), an ion foreshock must have formed in the prenoon sector, and it is likely that transmission of upstream waves into the magnetosphere occurred primarily through the morning flank of the magnetopause.

Figure 1e shows the upstream wave frequency f_{UW} given by equation (1) for the IMF measured by THEMIS C. The frequency is plotted only if $\theta_{xB} < 45°$, considering statistical studies reporting diminished magnetospheric

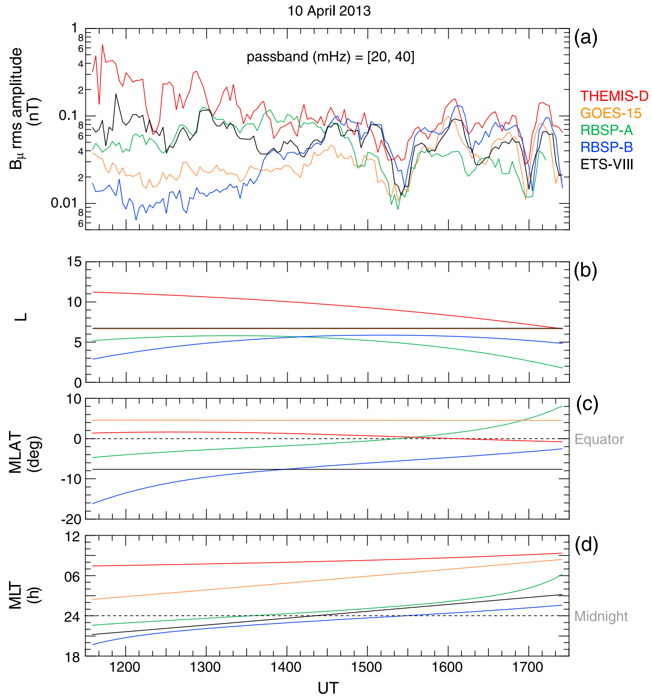

Figure 2. (a) Root-mean-square amplitudes of the B_μ components in the 20 to 40 mHz band at five spacecraft located within the magnetosphere. The colors indicate the source spacecraft. (b–d) Magnetic coordinates of the five spacecraft.

Pc3-Pc4 ULF wave power under large θ_{xB} [*Greenstadt and Olson*, 1976; *Takahashi et al.*, 1984]. The predicted frequency is mostly in the range 20–40 mHz.

Figures 1f–1j show the dynamic spectra of the B_μ components at the five spacecraft located within the magnetosphere. The spectra are generated from the Fourier transform of data contained in a 15 min moving window. The trend, a quadratic function fitted to the time series data by the least squares method, is removed, and the spectra are smoothed by taking 3-point running averages in the frequency domain. This method was used to generate other dynamic spectra presented in this paper.

The dynamic spectra indicate that each spacecraft detected oscillations with frequencies close to the predicted upstream wave frequency. At THEMIS D, which was located closest to the model magnetopause, compressional Pc3 waves are visible after 1400 UT at frequencies above 15 mHz. Prior to this time, there are strong irregular variations, which are caused by the entry of the spacecraft into the magnetopause boundary layer. The boundary layer variations dominate the dynamic spectra and mask the compressional Pc3 waves which may have been present before 1400 UT. At the other spacecraft, compressional Pc3 waves are more clearly visible throughout the 6 h interval as spectral enhancements in the 20 to 40 mHz band. We attribute the strong low-frequency power at ETS-VIII, seen from 1130 UT to ~1400 UT, to compressional Pc5 waves [*Barfield and McPherron*, 1972] most likely generated by ions injected during a small substorm that started at ~1100 UT (see Figure 3b).

The global nature of the Pc3 waves can be deduced from the overall similarity of amplitude modulations observed by multiple spacecraft. For example, the waves disappeared at ~1520 UT at all spacecraft. At this time, the IMF cone angle (Figure 1c) did not vary much, but the azimuthal angle (Figure 1d) became close to 180°, which means that a quasiparallel shock was formed at high magnetic latitude, where transmission of upstream waves into the magnetosphere may not be effective.

As another demonstration of the global nature of the compressional Pc3 waves, we show in Figure 2 the amplitude of the waves at the five spacecraft in the magnetosphere (Figure 2a) along with the magnetic coordinates of the spacecraft (Figures 2b–2d). The L maxima of RBSP A and RBSP B occurred at 1319 UT and 1513 UT, respectively, both very near midnight. RBSP A and RBSP B covered L ranges of 1.6–5.8 and 2.7–5.9, respectively. The amplitudes are root-mean-square (RMS) values obtained by taking the square root of the

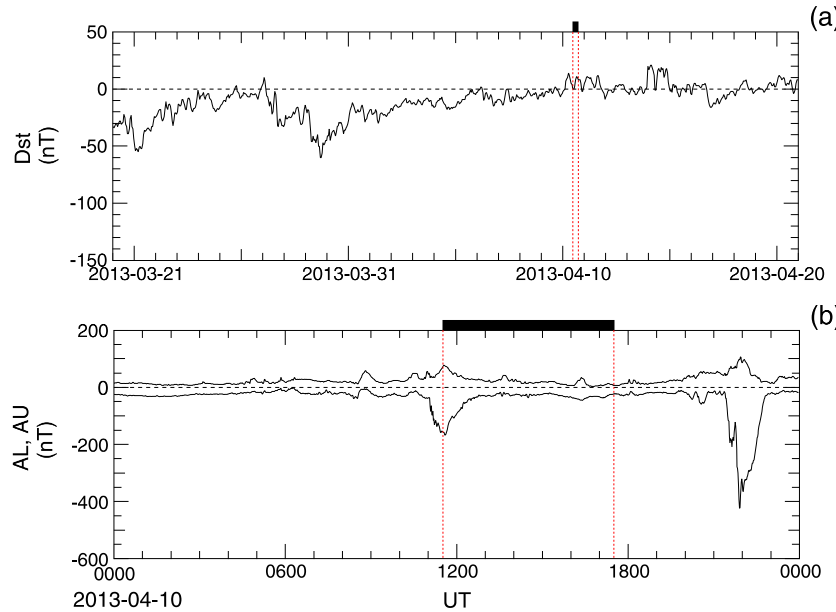

Figure 3. Geomagnetic activity indices covering the 6 h interval studied in the present paper, marked by black horizontal bars and vertical dashed lines. (a) *Dst* index. (b) Auroral electrojet indices *AU* and *AL*.

integral from 20 to 40 mHz of the B_μ power spectra that are computed in a 10 min moving data window. Except at THEMIS D, which detected oscillations associated with the magnetopause boundary layer during the first half of the interval shown, the amplitudes are below 0.15 nT. The amplitudes vary significantly, and many of the variations occur simultaneously at multiple spacecraft, indicating that the waves are not localized. In particular, the amplitude modulations occurring after 1500 UT are very similar among the five spacecraft.

The wave amplitude also depends on the spacecraft position. For example, from 1130 UT to 1330 UT, the amplitude at RBSP B is much lower than at RBSP A or ETS-VIII, although these spacecraft were all located on the nightside and were not far apart from each other. We believe that the larger distance of RBSP B from the magnetic equator (see Figure 2c) is the reason for the lower amplitude at this spacecraft. Equatorial confinement of compressional magnetic oscillations has been theoretically discussed by *Lee* [1996]. The amplitude should also depend on *L*. We examine the *L* dependence of the amplitude in section 4.2 in relation to the radial profile of the electron density.

The compressional Pc3 waves were observed when geomagnetic activity was low, making it unlikely that the waves were excited within the magnetosphere. Figure 3a shows that *Dst* was close to zero during the selected 6 h interval, meaning a very weak ring current. Figure 3b shows that the waves occurred following weak substorm activity that began at ∼1100 UT and recovered by ∼1300 UT after producing an AL minimum of −167 nT. There was no obvious substorm activation between 1130 UT and 1730 UT. Under these circumstances, it is reasonable to assume that the compressional Pc3 waves were not excited by processes occurring in the near-Earth magnetotail. Pi2 pulsations may be excited when the *AL* index does not exhibit strong changes [*Kim et al.*, 2005], but these Pi2 pulsations tend to have periods longer than 100 s [*Kwon et al.*, 2013], which is much longer than that (∼30 s) of the compressional Pc3 waves reported here.

4. Wave Properties

In this section we use various time series analysis techniques to determine the physical properties of the compressional Pc3 waves.

4.1. Waveforms and Spectra

Figure 4 shows 30 min snapshots of B_μ waveforms (Figure 4b) and the corresponding power spectra (Figure 4c) for the five spacecraft located in the magnetosphere (Figure 4a). The time resolution of the magnetometer data used for this figure is 0.5 s (GOES-15 and ETS-VIII), 1 s (RBSP), or 3 s (THEMIS D). To suppress high-frequency ($f > 40$ mHz) noise lines caused by satellite spin (RBSP) or heater currents (ETS-VIII) in the time series plots,

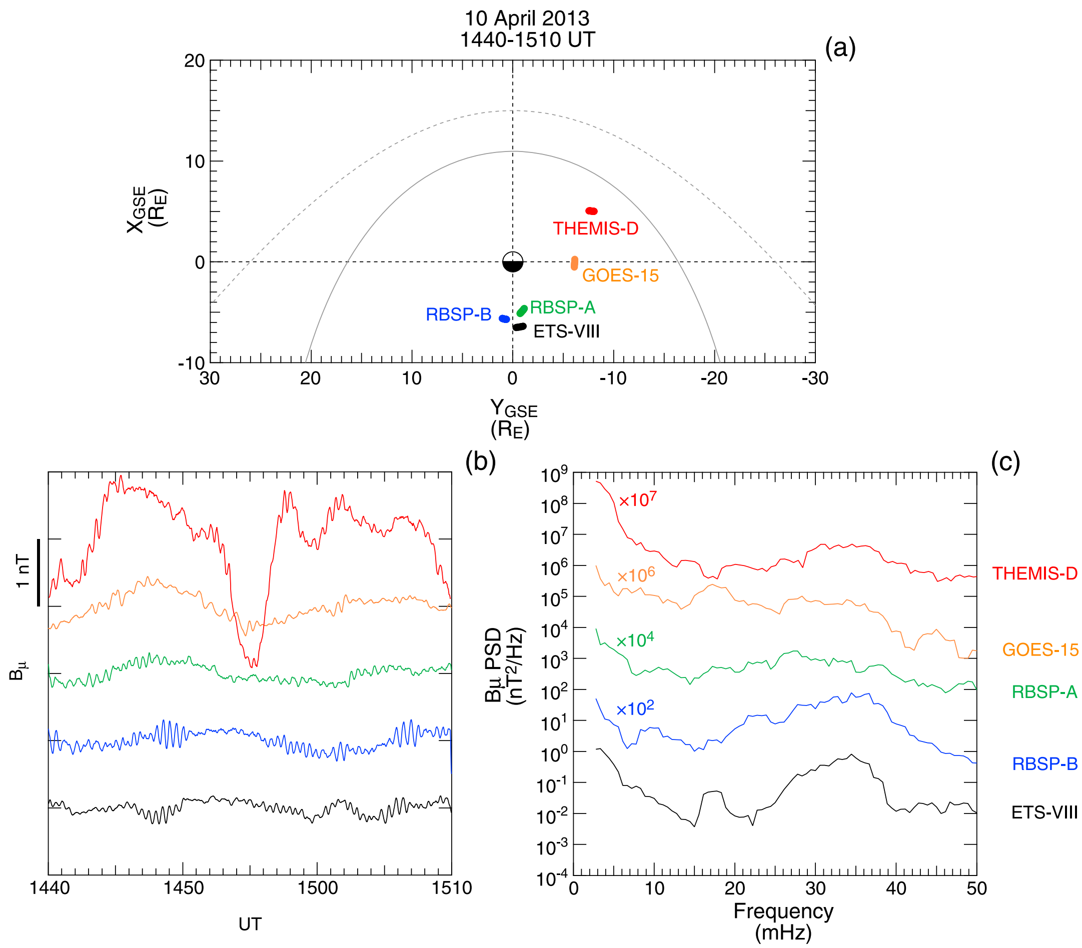

Figure 4. Comparison of B_μ oscillations at five spacecraft during a 30 min interval of compressional Pc3 waves. (a) Spacecraft positions in the GSE equatorial plane. (b) Time series plots of the B_μ components. For each spacecraft, slow variations have been removed by subtracting the best fit quadratic function from the original time series. (c) Power spectra computed from the time series. The spectra were smoothed by taking 5-point averages, and a factor of 10^1 or 10^2 offsets along the vertical axis are added between spacecraft.

we have smoothed the data by taking boxcar running averages with the boxcar length of 17 s for ETS-VIII and 11 s for RBSP. For consistency, data from THEMIS and GOES were also smoothed by 11 s boxcar averaging. In addition, we have suppressed near-dc variations by removing a quadratic function that is fitted to the original time series using the least squares method. Note that the power spectra were computed using the original time series without boxcar averaging. During the selected 30 min interval, THEMIS D was located at $L \sim 9.3$ and MLT ~ 8.3 h. GOES-15 was located at $L = 6.7$ and MLT ~ 6.0 h. RBSP A, RBSP B, and ETS-VIII were very close to midnight and maintained a triangular formation with relative distances in the range $1.6-2.2R_E$.

At each spacecraft, the B_μ time series exhibits slow variations that we attribute to solar wind dynamic pressure variations and fast oscillations that are the Pc3 waves we are interested in. The Pc3 waves have very low amplitudes, only a fraction of 1 nT, but they are clearly detected by each spacecraft, as was already seen in the dynamic spectra presented in Figure 1. Pc3 waves appear in wave packets lasting a few minutes, but the timing of the packets does not exactly match between spacecraft. Another notable feature is that the amplitude does not differ much between dayside (THEMIS D) and nightside (RBSP A, RBSP B, and ETS-VIII), and there are even instances (e.g., 1450 UT) when the amplitude is much larger at RBSP B ($L = 5.9$, MLT = 23.6 h) than at THEMIS D ($L = 9.4$, MLT = 8.2 h) or GOES-15 ($L = 6.7$, MLT = 5.7 h). Overall, the waves produce a broad spectral enhancement approximately between 20 and 40 mHz. The spectra at GOES-15 and ETS-VIII exhibit a peak

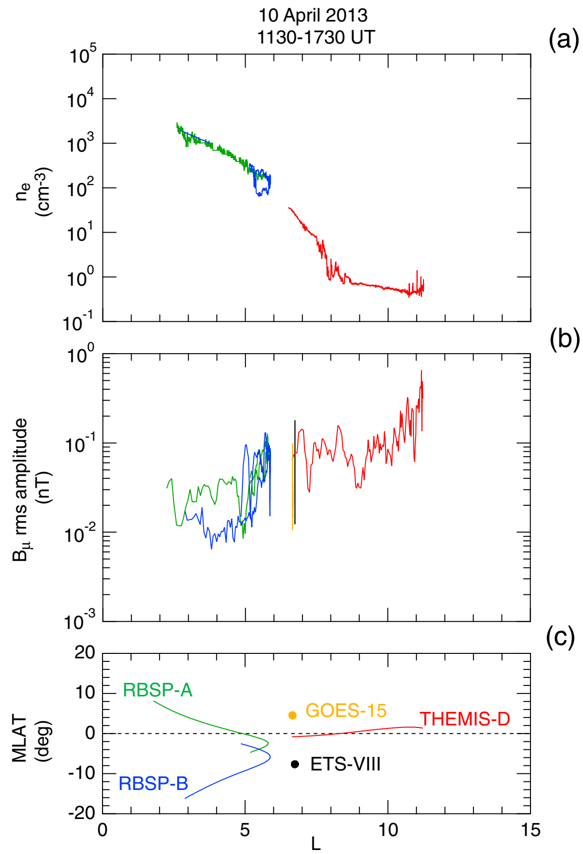

Figure 5. Quantities at five spacecraft for 1130–1730 UT plotted as a function of L of the spacecraft. The source spacecraft are shown by different colors as marked in Figure 5c. (a) Electron density at RBSP A (from plasma wave spectra), RBSP B (from spacecraft potential) and THEMIS D (from spacecraft potential) L. (b) Root-mean-square amplitude of the B_μ component. (c) Magnetic latitude.

at 17 mHz, which might be related to field line resonance as discussed by *Takahashi et al.* [2015b].

4.2. Pc3 Amplitude and Electron Density

Previous spacecraft studies reported that the plasmapause is a site of shielding [*Hartinger et al.*, 2010], trapping [*Takahashi et al.*, 2010], or amplification [*Clausen and Glassmeier*, 2014] of MHD fast-mode waves. *Takahashi et al.* [2005] discussed the possibility that nightside Pc4 waves detected on the ground are plasmaspheric cavity-mode waves. These studies motivate us to examine the relationship between the plasma density and the Pc3 waves. Figure 5 presents the L profiles of electron density (Figure 5a), B_μ amplitude (Figure 5b), and MLAT at each spacecraft for 1130–1730 UT.

The density data from THEMIS D indicate that the outer edge of the plasmapause, where the density gradient becomes small, was located at $L \sim 8$. This is far outside the normal range $L = 3–5$ [e.g., *Moldwin et al.*, 2002], but a distant plasmapause is not unusual during quiet times [*Kwon et al.*, 2013]. It is difficult to define the inner edge of the plasmapause because of the data gap at $L \sim 6$. However, it is clear that both RBSP A and RBSP B were within the plasmasphere because the density at these spacecraft was higher than 70 cm^{-3}.

Because the B_μ amplitude depends on UT as well as on MLT and MLAT, its L profile for each spacecraft is not a simple monotonic function (Figure 5b). The vertical lines at $L \sim 6.7$, which come from the geostationary satellites GOES-15 (MLAT = 5°) and ETS-VIII (MLAT = −8°) and span 0.01–0.2 nT, are a measure of how the amplitude varies with UT and/or MLT. As noted in Figure 2, the amplitude at RBSP B is substantially lower than at RBSP A, possibly because the former had a larger distance from the magnetic equator. At RBSP A, which stayed within 10° of the magnetic equator, the amplitude was in the range 0.01–0.05 nT at $L < 5$. This is ∼30% of the amplitude 0.03–0.2 nT detected by THEMIS D on the dayside near the outer edge of the plasmasphere and very close to the magnetic equator (|MLAT| < 2°)

Data plotted in Figure 5 do not provide sufficient information regarding the occurrence of cavity-mode resonance. Previous studies presented observationally determined radial amplitude and phase structures of ULF waves as evidence of the mode. For example, the B_μ component of the mode should exhibit an amplitude minimum and a 180° phase shift at the L shell of a node. Nightside observations of Pi2 pulsations [*Takahashi et al.*, 2003a] and a dayside observation of a Pc4 wave [*Takahashi et al.*, 2010] provided this evidence, and the node was found near the plasmapause in these studies. In Figure 5b, the L profile of the amplitude is highly variable, which makes it impossible to identify a node.

4.3. Interspacecraft Cross-Spectral Analysis

Propagation phase delay and coherence length of ULF waves can be studied by cross-spectral analysis of data from two spacecraft [e.g., *Takahashi et al.*, 2015a]. In the present study, we have three nightside spacecraft that maintained short distances from each other for an extended period. This orbital configuration allows us

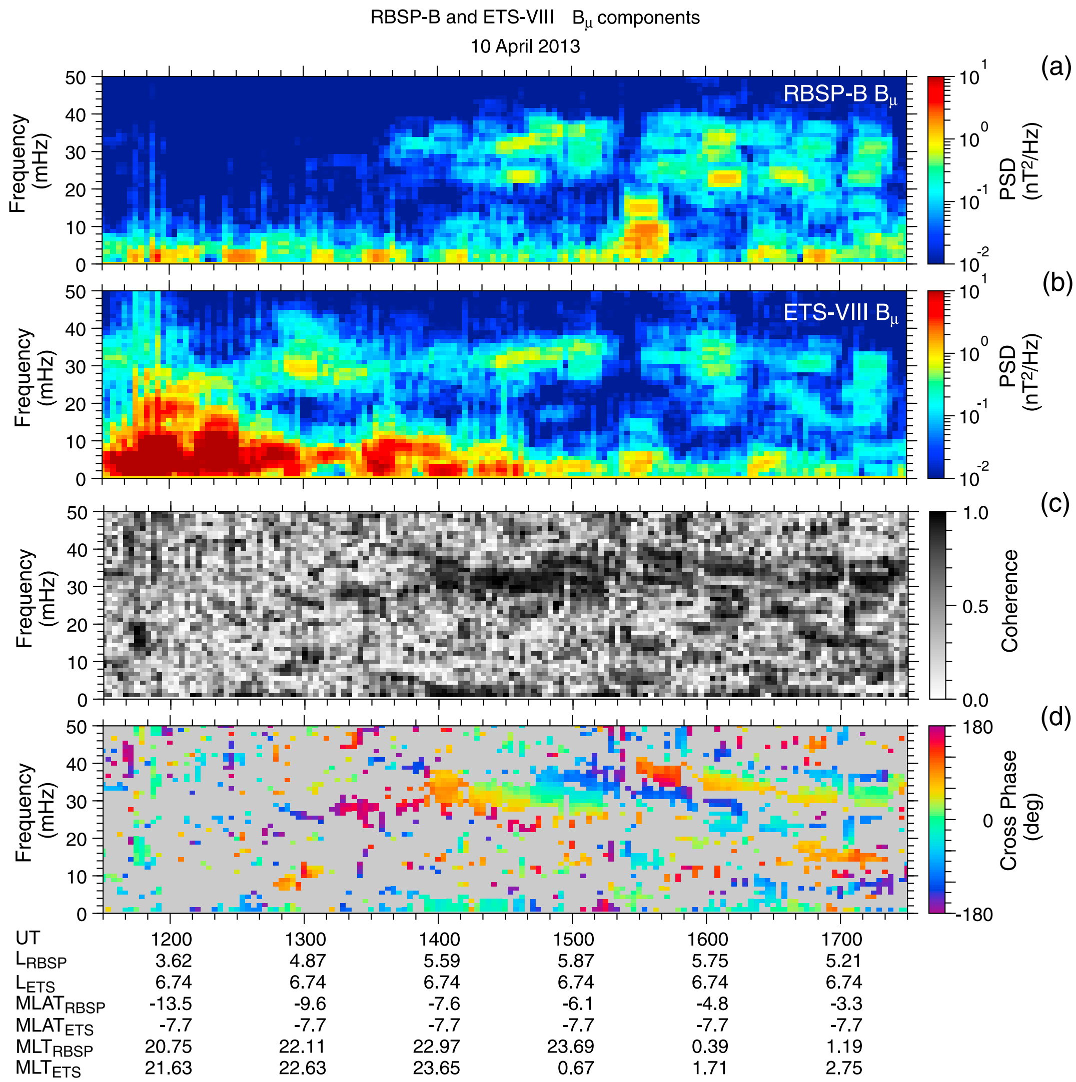

Figure 6. Dynamic display of spectral parameters computed from the B_μ time series at RBSP B and ETS-VIII. The magnetic coordinates of the spacecraft are shown at the bottom. (a) Power spectral density at RBSP B. (b) Power spectral density at ETS-VIII. (c) Coherence. (d) Cross phase.

to obtain information on how the compressional Pc3 waves were propagating. Figure 6 dynamically displays spectral parameters computed from the B_μ components at RBSP B and ETS-VIII. From 1330 UT to 1720 UT, when RBSP B was outside $L \sim 5$, the spectra at RBSP B (Figure 6a) and ETS-VIII (Figure 6b) are very similar and the coherence (Figure 6c) is elevated in the band occupied by the Pc3 waves. This indicates that the coherence length of the waves is at least of the order of the spacecraft separation, 0.9–1.8 in L and 0.6–1.6 h in MLT.

The cross-phase spectra (Figure 6d) exhibit a pattern that depends on both UT and frequency. If we follow the cross phase at 30 mHz (the center of the band occupied by the compressional Pc3 waves) along the time axis, we find that the color changes from orange at ~1400 UT to yellow/green at ~1500 UT and then to blue at ~1600 UT. A similar color transition is seen along the frequency axis at each time step. Qualitatively, the same cross-phase pattern is found in the cross-phase spectra generated from the RBSP A and ETS-VIII data.

To learn more about the propagation of the compressional Pc3 waves, we display in Figure 7 the cross-phase value at 30 mHz by the color of a pixel moving in the ΔMLT $-$ ΔL plane, where $\Delta \text{MLT} = \text{MLT}_{\text{ETS}} - \text{MLT}_{\text{RBSP}}$ and $\Delta L = L_{\text{ETS}} - L_{\text{RBSP}}$, respectively. A 15 min data window is used to calculate the cross phase, and the results are shown at 7.5 min intervals. The cross-phase value is shown only when the coherence is higher than 0.7.

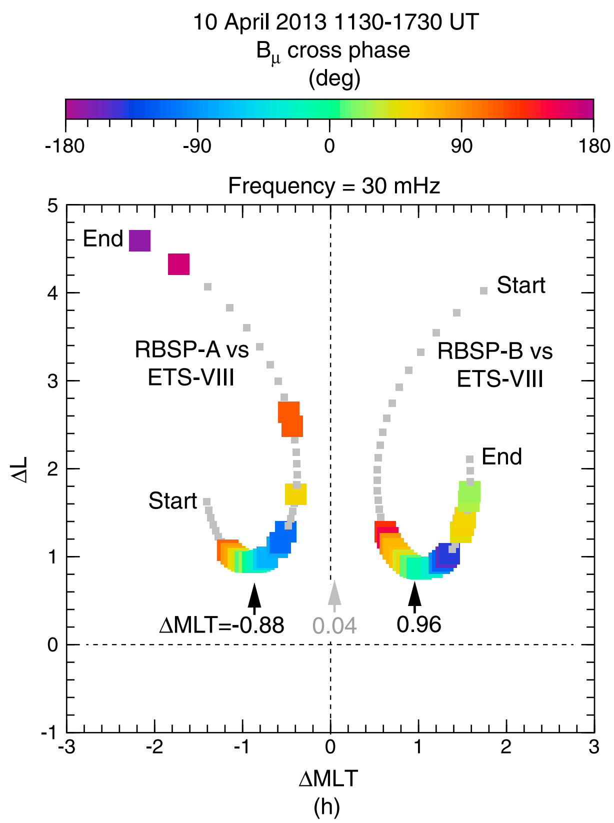

Figure 7. Color display of the cross phase between the B_μ components at RBSP and ETS-VIII evaluated at 30 mHz and plotted as a function of the spacecraft relative distance in MLT and L, denoted ΔMLT and ΔL, respectively. The cross-phase values are shown only if the B_μ coherence is higher than 0.7 at the selected frequency. See text for the explanation of the arrows.

A small gray square is plotted when the coherence is lower. The string of data points on the left comes from the pair of RBSP A and ETS-VIII, and the one on the right comes from the pair of RBSP B and ETS-VIII. The data points labeled "Start" and "End", respectively, indicate the first and last samples in the UT interval 1130–1730.

There are a few points we learn from Figure 7. First, if we use the 0.7 coherence value as the threshold, a common wave signal is easily detected at the ETS-VIII spacecraft and one RBSP spacecraft when they are separated in L by less than 2 and in MLT by less than 1.5 h. Second, within this domain of high coherence, the pixel color varies significantly, meaning that any cross-phase value between −180° and 180° is possible. However, the colors do not appear randomly. Instead, moving from left to right along $\Delta L \sim 1$, which corresponds to time periods when RBSP were near their apogees ($L \sim 5.8$), we find that the color changes from red to green and then to blue over a ΔMLT span of ∼1 h. This pattern is seen for both spacecraft pairs and can be explained by westward or duskward propagation of the oscillations.

To describe the wave propagation quantitatively, let us use the azimuthal phase velocity V_ϕ, azimuthal wavelength λ_ϕ, and dimensionless azimuthal wave number m [e.g., *Green*, 1976]. These parameters are related to each other and to the wave frequency f as

$$\lambda_\phi = \left(\frac{2\pi L R_E}{|m|}\right), V_\phi = \lambda_\phi f, \tag{2}$$

where L is evaluated at the position of the spacecraft. We define m to be positive for eastward propagating waves to be consistent with longitude (ϕ) being measured positive eastward.

We use the cross-phase analysis shown in Figure 7 to determine m and then use equation (2) to determine λ_ϕ and V_ϕ. In Figure 7, zero cross phase (marked by a black arrow) occurs at ΔMLT = −0.88 h for the pair of RBSP A and ETS-VIII and at ΔMLT = 0.96 h for the pair of RBSP B and ETS-VIII. Because the cross phase goes through a ∼360° variation over a ΔMLT range of ∼1 h for each spacecraft pair, it is reasonable to assume that one azimuthal wavelength spans ∼1 h in longitude. This means that we have two wavelengths between ΔMLT = −0.88 h and ΔMLT = 0.96 h and that zero cross phase occurs at the midpoint ΔMLT = 0.04 h, as marked by a gray arrow in Figure 7. Two wavelengths over a ΔMLT range of 1.84 h (= 0.96 − (−0.88)) and westward phase propagation translate to $m = -26$. From this m value, we get $\lambda_\phi = 8900$ km and $V_\phi = 270$ km/s, if we choose $L = 5.8$ to represent measurements at the RBSP apogee.

The same velocity applies not only to $f = 30$ mHz but also to other frequencies within the band occupied by the compressional Pc3 waves. Figure 8 shows spectral parameters computed from the B_μ components at RBSP B and ETS-VIII for 1440–1510 UT. The coherence exceeds 0.7 between 28 and 37 mHz (Figure 8b), and in this band the cross phase decreases linearly (Figure 8c), which corresponds to the color shift along the frequency axis that is seen in Figure 6d. The straight line in Figure 8c, which is fitted to the cross-phase data

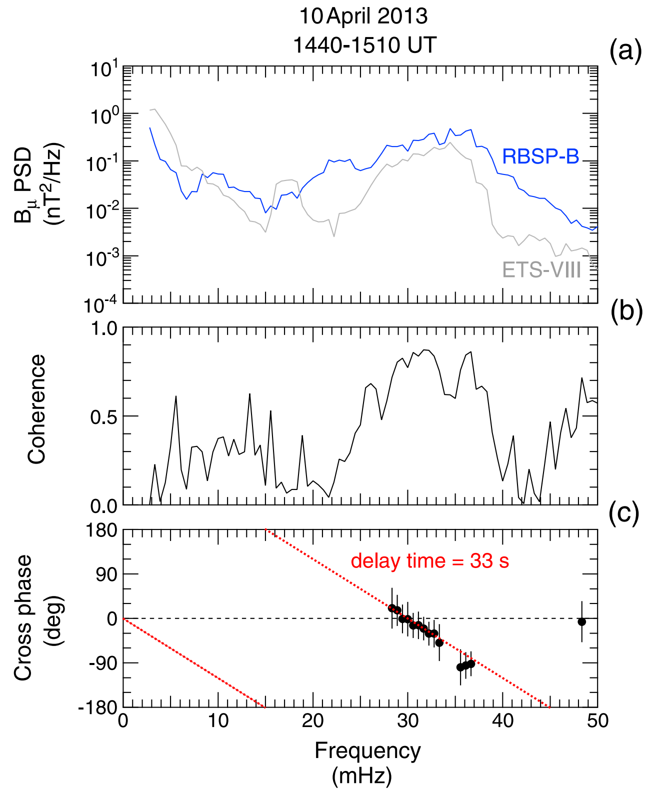

Figure 8. Frequency domain properties of the B_μ components at RBSP B and ETS-VIII for 1440–1510 UT on 10 April 2013. (a) Power spectra, repeated from Figure 4c. (b) Coherence. (c) Cross spectra shown at frequencies with coherence higher than 0.7. The vertical bars indicate the 95% confidence intervals described by *Green* [1976]. The red-dotted line gives cross phase for a signal propagating from ETS-VIII to RBSP B with a delay time of 33 s.

points and forced to intersect zero at $f = 0$, corresponds to a delay time of 33 s from ETS-VIII to RBSP B. This delay corresponds to the delay of the wave packets from ETS-VIII to RBSP B that is visible in Figure 4b. At 1455 UT, which is the middle of the 30 min interval considered, the spacecraft were separated by 5600 km in the radial direction and 9200 km in the azimuthal direction. If we attribute the 33 s delay time to purely azimuthal propagation, then the propagation velocity is 280 km/s, which is practically identical to the velocity determined from the phase delay at 30 mHz shown in Figure 7.

We infer that the wave phase varied little along L. While inspecting Figure 7, we inferred that zero cross phase occurred at (ΔMLT, ΔL) = (0.04 h, ∼1). By interpolation of zero cross phase at (−0.88 h, ∼1) and (0.96 h, ∼1), we estimate the cross phase at (0, ∼1) to be $\sim -10°$. Now noting that the cross phase is always zero at the origin (ΔMLT, ΔL) = (0, 0) (consider ETS-VIII versus ETS-VIII cross phase), we infer that the phase changes only by ∼10° over an L distance of ∼1 or a radial distance of ∼6000 km. By contrast, the phase changes by 360° over a similar azimuthal distance. It appears that the waves were propagating nearly purely azimuthally. Alternatively, the small variation of phase with L could be attributed to radially standing modes such as cavity/waveguide modes [e.g., *Wright*, 1994] or to radially evanescent modes.

4.4. Relationship Between Electric and Magnetic Fields

Until now, we examined only the compressional component of the magnetic field. We now use all field components available from RBSP A to examine the polarization and propagation mode of the waves. Figure 9 shows the electron density (Figure 9a), the power spectra of two components of the electric field and three components of the magnetic field (Figures 9b–9f), and cross phase (Figure 9g) between $E_{y\mathrm{MGSE}}$ and B_μ. The electric field was measured using two pairs of spherical probes mounted at the ends of four wire booms placed in the spacecraft spin plane. The measured components have been rotated into the Modified Geocentric Solar Ecliptic (MGSE) coordinates, in which $\mathbf{e}_{x\mathrm{MGSE}}$ is the direction of the spin axis, $\mathbf{e}_{y\mathrm{MGSE}}$ is duskward, and $\mathbf{e}_{z\mathrm{MGSE}}$ is northward. By definition, the spin plane measurements do not provide the $E_{x\mathrm{MGSE}}$ component.

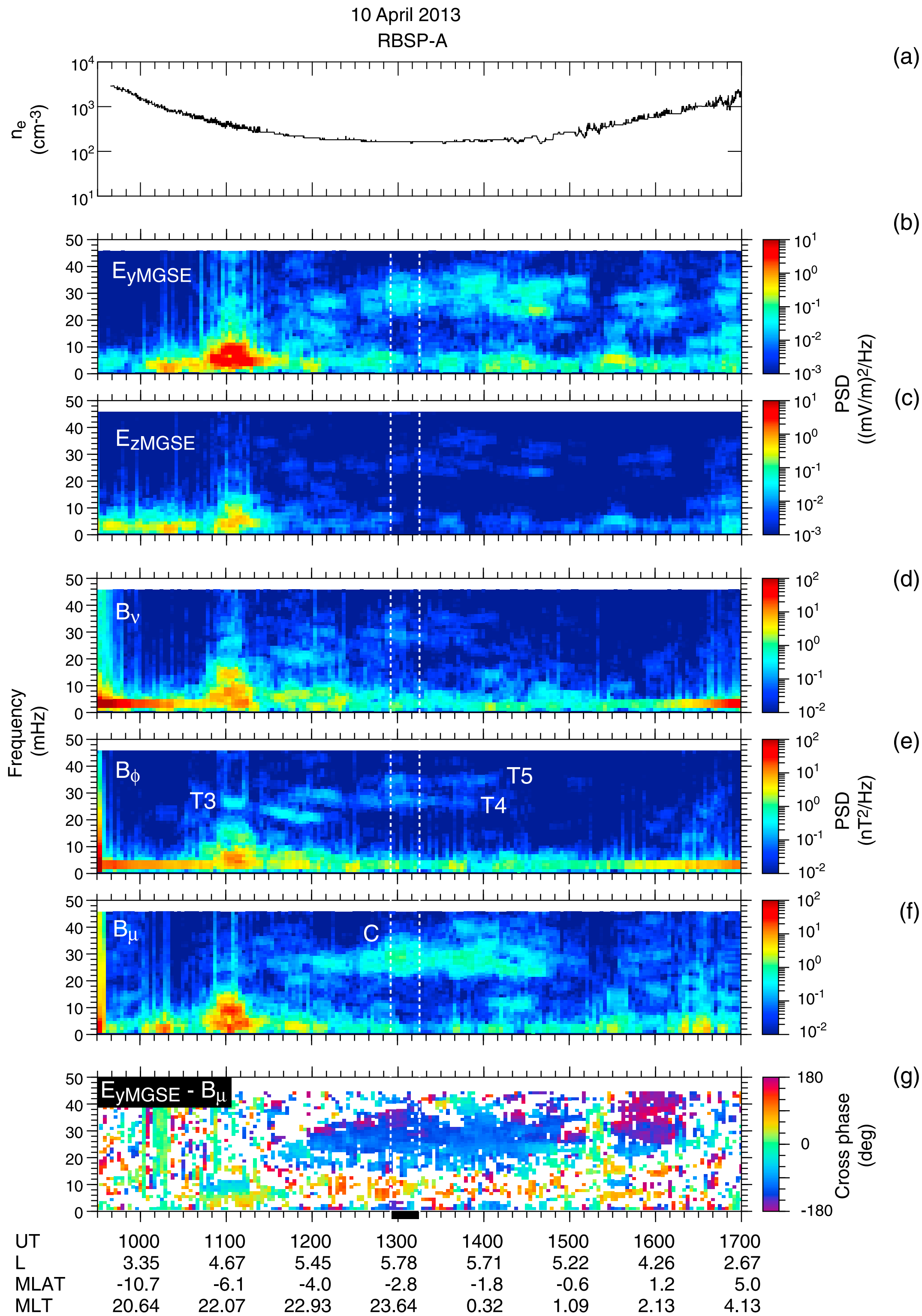

Figure 9. RBSP A data covering $L > 2.7$ on the orbit that contains the compressional Pc3 wave event. The vertical dashed lines mark the 20 min interval that is used for generating Figure 10. (a) Electron density. (b, c) Dynamic power spectra of the electric field $E_{y\mathrm{MGSE}}$ and $E_{z\mathrm{MGSE}}$ components in the MGSE coordinates. (d–f) Dynamic spectra of the magnetic field components in the model field aligned coordinates. (g) Cross phase between $E_{y\mathrm{MGSE}}$ and B_μ.

We can estimate $E_{x\mathrm{MGSE}}$ using the $\mathbf{E}\cdot\mathbf{B} = 0$ assumption when the background magnetic field makes a large angle from the spin plane, but this condition was not satisfied during the wave event. The magnetic field is given in a local coordinate system in which $\mathbf{e}_\mu$ is along the T89c model magnetic field [*Tsyganenko*, 1989], $\mathbf{e}_\phi$ is perpendicular to $\mathbf{e}_\mu$ and directed eastward, and the outward component $\mathbf{e}_\nu$ completes the right-handed orthogonal system $\nu - \phi - \mu$. B_μ is essentially the field magnitude, and a perturbation in this component means magnetic field compression. RBSP A was located within 1 h of midnight when the compressional Pc3 waves were most intense. At this location, $-E_{y\mathrm{MGSE}}$ is approximately equal to the eastward component (E_ϕ) in the $\nu - \phi - \mu$ coordinates and represents poloidal-mode waves. Meanwhile, $E_{z\mathrm{MGSE}}$ is close to the component parallel to the background magnetic field (E_μ).

The magnetic field spectra exhibit broadband 20 to 40 mHz oscillations (labeled "C," for compressional) only in the B_μ component. This implies that the oscillations are associated with fast-mode waves propagating nearly perpendicular to the background magnetic field. The B_ϕ spectra exhibit discrete spectral lines labeled "T3," "T4," and "T5." These are most likely caused by the coupling of the compressional Pc3 waves with the third through fifth harmonics of toroidal-mode standing Alfvén waves through the field line resonance mechanism, a process that commonly occurs on the dayside [*Takahashi et al.*, 1984].

The $E_{y\mathrm{MGSE}}$ spectra, with power confined in the 20 to 40 mHz band, are very similar to the B_μ spectra, which indicates that compressional Pc3 waves accompany an electric field. Spectral power in the $E_{z\mathrm{MGSE}}$ component is low, which is expected because this component is nearly parallel to the ambient magnetic field and MHD waves do not produce parallel electric field perturbations. As mentioned above, we do not have measurements of $E_{x\mathrm{MGSE}}$ (nearly equal to $-E_\nu$), which would show oscillations if there were toroidal-mode standing Alfvén waves or fast-mode waves propagating perpendicular to the ambient magnetic field with a wave normal that has a finite azimuthal component.

Figure 9g shows $E_{y\mathrm{MGSE}} - B_\mu$ cross-phase values at frequencies with coherence higher than 0.7. In the band occupied by the compressional Pc3 waves, the coherence is high and the pixel color is mostly dark blue, which means that B_μ leads the $E_{y\mathrm{MGSE}}$ by one quarter to one third of a wave period if we neglect a $2n\pi$ ambiguity. High coherence and stable cross-phase is seen continuously from 1200 UT (~23 h MLT) to 1620 UT (~2 h MLT) with the exception of a gap at 1520 UT. This long duration suggests that there was a continuous transmission of wave energy from an external source region.

The relationship between $E_{y\mathrm{MGSE}}$ and B_μ can be examined more quantitatively in Figure 10, which shows 20 min time series and spectrum snapshots of the components. The selected time segment is 1255–1315 UT, which is marked in Figure 9 by vertical dashed lines. The temporal variations (Figures 10a and 10b) and the corresponding power spectra (Figure 10c) are very similar between $E_{y\mathrm{MGSE}}$ and B_μ. The spectra are enhanced between 20 and 40 mHz, and in this band, the $E_{y\mathrm{MGSE}}$ to B_μ power ratio is ~0.05 ((mV/m)/nT)^2 (Figure 10d) and the coherence exceeds 0.6 (Figure 10e). The cross phase changes with frequency from $\sim -90°$ at 22 mHz to $\sim -150°$ at 35 mHz (Figure 10f). At the frequency of 30 mHz, which was our focus in section 4.3, the cross phase is $-130°$. This means that the waves were neither purely propagating nor purely standing in the radial direction. The cross phase should be 0 or 180° for a propagating wave and $-90°$ or 90° for a standing wave [e.g., *Takahashi et al.*, 2003a].

The observed cross phase might be explained by radial reflection of fast-mode waves. In an inhomogeneous plasma, incident fast-mode waves will become evanescent at turning points that depend on the frequency and wavelength. *Lee* [1996] discussed this phenomenon using a box magnetosphere in which the magnetic field is directed along the z axis, x is the radial direction, and y is the azimuthal direction. Lee introduced a function g given by

$$g(x) = \frac{\omega^2}{V_A^2(x)} - k_y^2 - k_z^2. \tag{3}$$

For a given Alfvén velocity profile $V_A(x)$ and fixed wave numbers in the y direction, k_y, and the z direction, k_z, the turning point x_t such that $g(x_t) = 0$ is a function of frequency ω. In the region where a wave is radially evanescent, the amplitude decays exponentially with the radial distance from the turning point, whereas the phase does not change with x inward of the turning point. Accordingly, the cross phase is zero between oscillations that are measured at two radially separated locations (but at the same azimuth) within the region of evanescence [e.g., *Kim and Takahashi*, 1999]. Meanwhile, the wave retains the same wave azimuthal number k_y both inside and outside the turning point. Therefore, the cross phase between oscillations measured

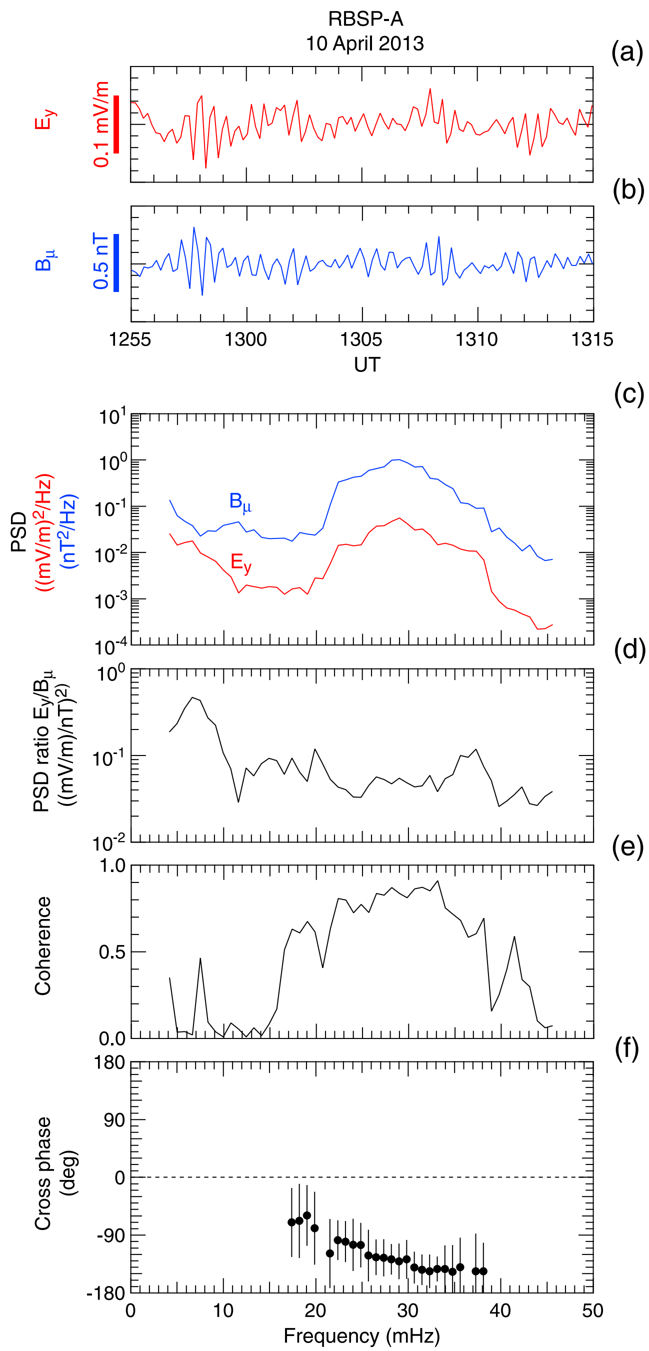

Figure 10. (a, b) RBSP A $E_{y\mathrm{MGSE}}$ and B_μ time series for the 20 min segment marked in Figure 9. (c–f) Spectral parameters calculated from the $E_{y\mathrm{MGSE}}$ and B_μ time series data. The cross phase is displayed only when the coherence is higher than 0.6.

by two azimuthally separated spacecraft in the region of evanescence would indicate a nonzero value that corresponds to k_y.

Waves in the magnetosphere are not likely to be represented by a single-frequency and a single-wave vector. Rather, waves can be envisioned as an ensemble of disturbances with a range of frequencies and a range of wave vectors. Even at a single frequency (that is, a single Fourier component that we can obtain from a data segment of finite length), there could be multiple k_y values. Depending on the value of k_y, the wave may or may not be radially evanescent. When evanescent and radially propagating waves simultaneously exist at a single frequency, the E_y and B_z components in the box magnetosphere (corresponding to the $E_{y\mathrm{MGSE}}$ and

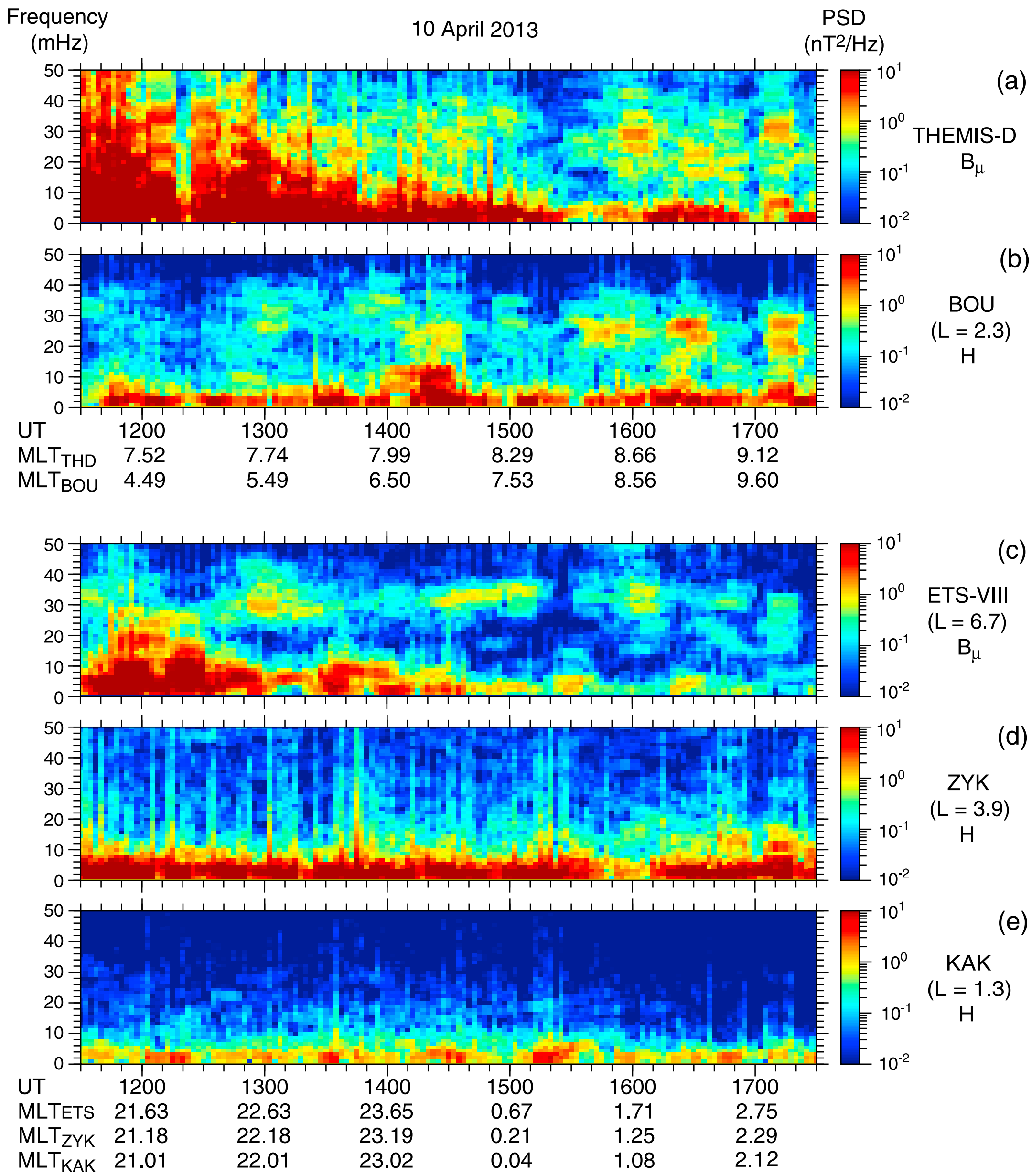

Figure 11. (a, b) Comparison of dayside observations of B_μ oscillations in the magnetosphere (THEMIS D, repeated from Figure 1f) and H oscillations on the ground at Boulder (BOU). The L value and magnetic local time of each observatory are given at the bottom and on the right, respectively. (c–e) Comparison of nightside observations in the magnetosphere (ETS-VIII, repeated from Figure 1j) and on the ground at Zyryanka (ZYK) and Kakioka (KAK).

B_μ components in the real magnetosphere) will not oscillate exactly in phase or out of phase (propagating waves) or in quadrature (standing or evanescent waves). This mixture of wave components might explain the cross-phase value in Figure 10f, which changes with frequency from −60° to −150°.

Although the above analysis indicates that waves are not simply propagating in the radial direction, the amplitude ratio between $E_{y\mathrm{MGSE}}$ and B_μ is close to what we expect for propagating fast-mode waves. In a cold plasma, the phase velocity of fast-mode waves is equal to the Alfvén velocity V_A $(= B(\mu_0\rho)^{-1/2})$, where B is the magnitude of the background magnetic field, μ_0 is the permeability of free space, and ρ is the mass density. If a fast-mode wave propagates radially perpendicular to the background magnetic field, it produces perturbations in the compressional component of the magnetic field δB_μ and the azimuthal component of the electric field δE_ϕ. These are related to the phase velocity as $V_A = \pm\delta E_\phi/\delta B_\mu$, where the positive (negative) sign means outward (inward) propagation. During the time interval covered by Figure 10, the magnetic field magnitude at RBSP A was ∼145 nT and the electron density was ∼170 cm^{-3}. For an all-proton plasma, which is a good approximation in a quiet time magnetosphere [e.g., *Takahashi et al.*, 2015a], these values give a local fast-mode velocity of 250 km/s. In the presence of heavy ions, the velocity becomes lower. Meanwhile, we find the $E_{y\mathrm{MGSE}}$ to B_μ power ratio to be ∼0.05 ((mV/m)/nT)^2 (Figure 10d), which is equivalent to $\delta E_\phi/\delta B_\mu$∼0.2 ((mV/m)/nT) and to a phase velocity of ∼200 km/s. The good match between the velocities derived using different methods indicates that the observed waves were indeed fast-mode waves.

4.5. Observations on the Ground

Finally, we examine whether the compressional Pc3 waves propagated to the ground. Figure 11 compares dynamic spectra at THEMIS D and ETS-VIII and three ground stations located at Boulder (BOU, $L = 2.3$), Zyryanka (ZYK, $L = 3.9$), and Kakioka (KAK, $L = 1.3$).

On the dayside (Figures 11a and 11b) there is high degree of similarity between the B_μ spectra in the magnetosphere and the *H* spectra on the ground, despite the fact that the observations were made with *L* and MLT separations of 4.5 and 2.4 h, respectively. This indicates that the compressional waves propagated to the ground preserving their spectral contents, as has been reported in previous studies [*Clausen et al.*, 2009].

On the nightside, by contrast, there is little indication that the compressional waves propagated to the ground. The Pc3 waves that are clearly present in the ETS-VIII spectra (Figure 11c) are absent in the spectra at ZYK (Figure 11d) and KAK (Figure 11e). This is different from the cases reported by *Takahashi et al.* [2005] or *Ponomarenko et al.* [2010]. Although the amplitude of the Pc3 waves in the magnetosphere is only of the order of ∼0.1 nT, the ground magnetometers are sensitive enough to detect the waves if their ground-level amplitude is also ∼0.1 nT [*Takahashi et al.*, 2005].

5. Discussion

A general question regarding fast-mode waves in the magnetosphere is whether they are radially propagating or standing. Concerning fast-mode waves in the Pc3-Pc4 band, some studies considered that the waves are simply propagating [e.g., *Takahashi et al.*, 1994], while other studies considered the possibility of radially trapped modes [*Yumoto and Saito*, 1983; *Kim and Takahashi*, 1999]. A distinction between these wave types is that the former preserves the frequency from the source region to the point of observation, while the latter resonantly amplifies field perturbations at the frequencies of the cavity or waveguide eigenmodes.

The frequency of trapped (cavity) mode depends on the size of the cavity and the fast-mode velocity in it. Usually, the cavity is considered to be formed by the whole magnetosphere [*Kivelson et al.*, 1984] or by the plasmasphere [*McClay*, 1970], and the estimated fundamental frequency is a few millihertz for the former [e.g., *Samson et al.*, 1992] and 7–30 mHz for the latter [e.g., *Yeoman and Orr*, 1989]. From a frequency point of view, it is unlikely that our compressional Pc3 waves (∼30 mHz) are related to the whole magnetosphere cavity mode, but we cannot exclude the possibility that the plasmaspheric cavity mode played a role in controlling the properties of the waves.

We can estimate the fundamental frequency of the plasmaspheric cavity mode during our Pc3 wave event. The frequency depends primarily on the size of the plasmasphere. When the geomagnetic activity is lower, the plasmasphere will be larger and the frequency will be lower, because the fast-mode travel time between the inner and lower boundaries is longer. As shown in Figure 3, the *Dst* and *AE* indices indicate that the geomagnetic activity was low during the wave event. The *Kp* index also had low values between 1_- and 1_+. Consistent with this geomagnetic condition, THEMIS D crossed the outer edge of the plasmapause at a large distance $L \sim 8$, as shown in Figure 5a. The same figure shows that the inner edge of the plasmapause, which is commonly used to define the plasmapause distance [*Carpenter and Anderson*, 1992; *Moldwin et al.*, 2002], was located somewhere between $L = 5$ and $L = 6.5$, outside the average plasmapause. With such an expanded plasmasphere, the fundamental frequency of the plasmaspheric cavity mode is expected to be ∼10 mHz [*Yeoman and Orr*, 1989; *Takahashi et al.*, 2003a; *Kwon et al.*, 2013], much lower than the frequency, ∼30 mHz, of the observed compressional Pc3 waves. Therefore, it is unlikely that there was coupling between the compressional Pc3 waves and the fundamental plasmaspheric cavity mode.

There still remains a possibility that higher harmonics of the plasmaspheric cavity mode affected the properties of the compressional Pc3 waves. Numerical simulations routinely produce the higher harmonics [*Allan et al.*, 1986; *Lee and Lysak*, 1999; *Lee and Takahashi*, 2006], and spacecraft observations of the second harmonic in the 14–19 mHz range have been reported in association with Pi2 pulsations [*Takahashi et al.*, 2003b;

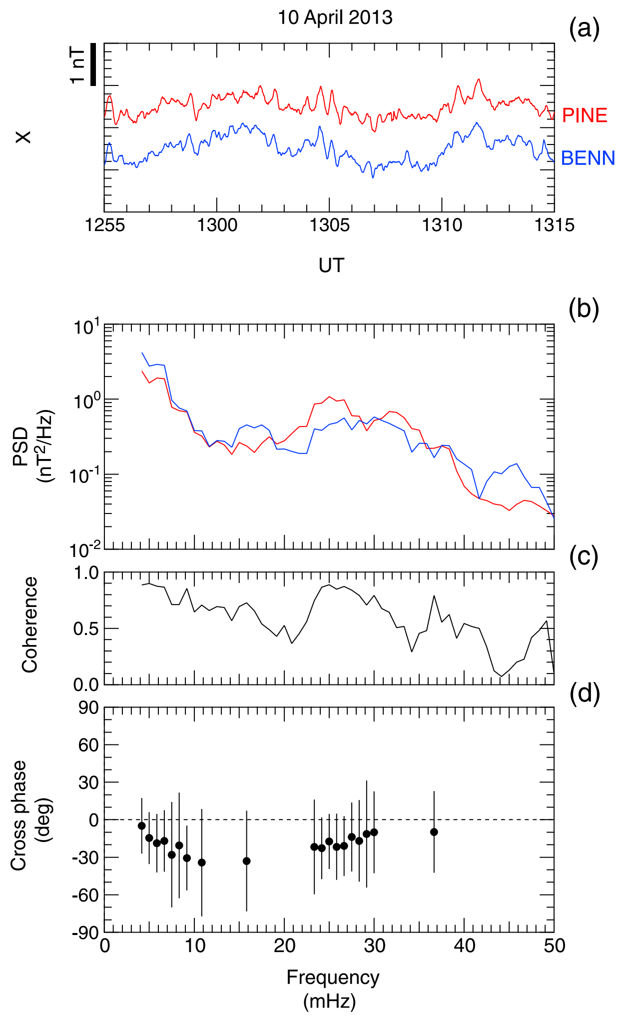

Figure 12. Comparison of magnetic field oscillations in the northward component observed on the ground at PINE and BENN. (a) Time series plots. (b) Power spectra computed from the time series data. (c) Coherence spectrum. (d) Cross-phase spectrum.

Luo et al., 2011]. It appears that the third or fourth harmonic of the plasmaspheric cavity mode had a frequency that was close to that of the compressional Pc3 waves. Accordingly, it is possible that the Pc3 waves were amplified within the plasmasphere via resonance with a higher harmonic of the cavity mode.

However, we argue that the plasmaspheric cavity-mode resonance did not play a major role in determining the spectral shape of the observed Pc3 waves. The main reason is the similarity in the B_μ spectrum seen in Figure 4c between THEMIS D, which was located on the dayside outside the plasmasphere, and RBSP B, which was located near midnight in the plasmasphere. At both locations, the spectrum shows a broad peak around 35 mHz. It is difficult to explain the spectral peak at THEMIS D by the plasmaspheric cavity mode because the higher harmonics of the mode are confined to the plasmasphere according to numerical simulations [e.g., *Lee and Takahashi*, 2006]. Instead, the spectral peak can be explained by fast-mode waves propagating from the external source region. This spectral component could be enhanced inside the plasmasphere if there is a cavity-mode frequency that matches it. However, this amplification needs not occur to explain the observation. Our interpretation of the Pc3 waves is similar to that of Pc5 waves that are driven by periodic variations of the solar wind dynamic pressure [*Kepko and Spence*, 2003].

We note that a different interpretation has been proposed for plasmaspheric Pi2 pulsations. In the cavity-mode Pi2 model [*Takahashi et al.*, 2003a, 2003b], the Pi2 frequency is established as a result of excitation of discrete-frequency cavity-mode oscillations by an impulsive or broadband disturbance propagating

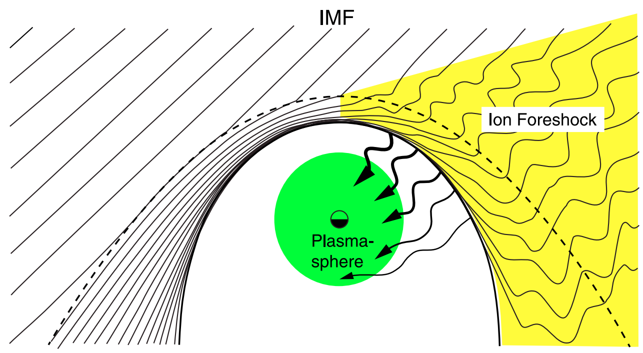

Figure 13. Schematic summary of the observations presented in the present paper. ULF waves are generated in the ion foreshock region. The waves enter the magnetosheath, impact the magnetopause, and propagate into the magnetosphere as fast-mode waves and enter the plasmasphere even on the nightside. The magnetic field lines are adapted from Figure 21 of *Spreiter et al.* [1966].

into the inner magnetosphere from the near-Earth magnetotail. In this case, the power spectrum differs significantly inside and outside the resonance cavity.

The absence of ground signatures of the compressional Pc3 waves in the midnight sector is somewhat puzzling. *Takahashi et al.* [2005] and *Ponomarenko et al.* [2010] reported ground observations of nightside Pc3-Pc4 waves of dayside origin, although they did not examine spacecraft data. It is possible that our waves had much lower intensity than those reported in previous studies. Our waves had amplitudes of the order of 0.1 nT in the equatorial magnetosphere, which is indeed very low. By contrast, plasmaspheric Pi2 waves, which are also fast-mode waves, have amplitudes of the order of 1 nT and are detected with similar amplitudes at ground stations located at $L < 2$ [*Takahashi et al.*, 1992].

Another reason for the absence of ground signatures of the compressional Pc3 waves may be ionospheric screening. With the $|m|$ value of ∼30, some degree of amplitude attenuation is expected below the ionosphere by the ionospheric screening effect [*Nishida*, 1978]. By contrast, Pi2 pulsations propagating to the inner magnetosphere have much lower $|m|$ values [*Sutcliffe and Yumoto*, 1991; *Nosé et al.*, 2003] and will not suffer ionospheric attenuation.

We examined magnetometer data from two ground stations close to BOU to infer the m number away from midnight, at dawn. Figure 12a shows the horizontal northward (X) components at Pine Ridge (PINE, magnetic longitude = 323.6°E, L = 2.7) and Bennington (BENN, magnetic longitude = 331.29°E, L = 2.6) for 1255–1315 UT. The power spectra computed from the time series data exhibit a broad peak at 30 mHz (Figure 12b), similar to the spectra at RBSP A shown in Figure 10 for the same time period. The coherence is higher than 0.7 at 23–30 mHz (Figure 12c), with a cross-phase value of about −20° at 24–27 mHz where the coherence peaks (Figure 12d). The negative cross phase indicates that the waves were propagating from BENN to PINE (tailward or westward). Because the stations are separated in longitude by 8°, the cross phase corresponds to $m \sim -2.5$. This low-m value implies that the ionospheric screening effect was low at ∼06 h MLT, where the ground observations were made.

The low m value at dawn can be explained by a model of wave generation and propagation illustrated in Figure 13. In this model, fast-mode waves are launched inward from the magnetopause primarily between dawn and dusk, where the impact of ULF waves generated in the foreshock region is the strongest for the given IMF orientation. Between dawn and noon, the fast-mode waves have a wave normal nearly perpendicular to the plasmapause (only the equatorial propagation is considered here). This propagation geometry translates to a small m number at dawn. Away from the local time of wave entry, the wave normal will acquire a large component tangential to the plasmapause. In Figure 13, the waves propagate almost purely azimuthally at midnight. This local time dependence can explain the large m number inferred from multisatellite observations near midnight.

6. Conclusions

In conclusion, we have provided clear evidence that fast-mode waves of upstream origin reach the midnight sector of the plasmasphere. The amplitude of the waves on the nightside is small, of the order of 0.1 nT, but their power spectra stand out from the background noise level in the 20 to 40 mHz band. Data from multiple spacecraft located in the solar wind, dayside magnetosphere, and nightside magnetosphere indicate that the frequency of the waves is consistent with their generation in the ion foreshock. In addition, the global coherence in overall amplitude variations indicates that the waves are fast-mode waves. Propagation in fast mode is also consistent with the relationship between electric and magnetic field perturbations and with the phase delay between spacecraft. Compressional ULF magnetic field oscillations on the nightside are usually attributed to waves excited on the nightside, most often in association with substorms. Our study demonstrates that this is not always the case. More study needs to be conducted to determine the degree that dayside sources contribute to ULF oscillations observed in the midnight sector.

Acknowledgments
Work at JHU/APL was supported by NASA grants NNX13AE02G and NNX14AB97G. M.D. Hartinger was supported by NSF AGS-1049403. Work at IKFIA Siberian Branch, Russian Academy of Sciences was partially supported by program "JSPS Core-to-Core Program, B. Asia-Africa Science Platforms" and the Russian Foundation for Basic Research (grants 15-45-05090 (MAV) and 15-45-05108 (BDG)). Work at Kyushu University was supported by MEXT/JSPS KAKENHI grant 15H05815. Data used in this study can be obtained by contacting the following sources: Van Allen Probes Science Operation Centers located at University of Iowa (http://emfisis.physics.uiowa.edu) and University of Minnesota (http://www.space.umn.edu/missions/rbspefw-home-university-of-minnesota) for RBSP; Space Science Laboratory, University of California, Berkeley (http://themis.ssl.berkeley.edu), for THEMIS, including the BENN and PINE ground magnetometers; NOAA National Geophysical Data Center (http://satdat.ngdc.noaa.gov) for GOES; Japan Aerospace Exploration Agency, Japan (contact: koga.kiyokazu@jaxa.jp), for ETS-VIII; USGS (http://geomag.usgs.gov/products/downloads.php) for the Boulder magnetometer; Space Environment Research Center, Kyushu University (http://magdas.serc.kyushu-u.ac.jp), for the Zyryanka magnetometer; and Kakioka Magnetic Observatory (http://www.kakioka-jma.go.jp) for the Kakioka magnetometer. Peter Chi and NSF grant ATM-0245139 are acknowledged for the use of the BENN magnetometer data. S. Mende, C.T. Russell and NSF grant AGS-1004814 are acknowledged for the use of the PINE magnetometer data.

References

Allan, W., E. M. Poulter, and S. P. White (1986), Hydromagnetic wave coupling in the magnetosphere-plasmapause effects on impulse-excited resonances, *Planet. Space Sci.*, *34*(12), 1189–1220, doi:10.1016/0032-0633(86)90056-5.

Auster, H. U., et al. (2008), The THEMIS fluxgate magnetometer, *Space Sci. Rev.*, *141*, 235–264, doi:10.1007/s11214-008-9365-9.

Barfield, J. N., and R. L. McPherron (1972), Statistical characteristics of storm-associated Pc5 micropulsations observed at the synchronous equatorial orbit, *J. Geophys. Res.*, *77*(25), 4720–4733.

Bol'shakova, O. V., and V. Troitskaya (1968), Relation of the IMF direction to the system of stable oscillations, *Dokl. Akad. Nauk*, *180*, 343–346.

Carpenter, D. L., and R. R. Anderson (1992), An ISEE/whistler model of equatorial electron density in the magnetosphere, *J. Geophys. Res.*, *97*(A2), 1097–1108, doi:10.1029/91JA01548.

Chi, P. J., et al. (2013), Sounding of the plasmasphere by Mid-continent Magnetoseismic Chain (McMAC) magnetometers, *J. Geophys. Res. Space Physics*, *118*, 3077–3086, doi:10.1002/jgra.50274.

Clausen, L. B. N., and K.-H. Glassmeier (2014), Enhancement of ultralow frequency wave amplitudes at the plasmapause, *J. Geophys. Res. Space Physics*, *119*, 9113–9124, doi:10.1002/2014JA020072.

Clausen, L. B. N., T. K. Yeoman, R. C. Fear, R. Behlke, E. A. Lucek, and M. J. Engebretson (2009), First simultaneous measurements of waves generated at the bow shock in the solar wind, the magnetosphere and on the ground, *Ann. Geophys.*, *27*, 357–371, doi:10.5194/angeo-27-357-2009.

Fairfield, D. H. (1969), Bow shock associated waves observed in the far upstream interplanetary medium, *J. Geophys. Res.*, *74*(14), 3541–3553, doi:10.1029/JA074i014p03541.

Fairfield, D. H. (1971), Average and unusual locations for the Earth's magnetopause and bow shock, *J. Geophys. Res.*, *76*, 6700–6716, doi:10.1029/JA076i028p06700.

Green, C. A. (1976), The longitudinal phase variation of mid-latitude Pc3–4 micropulsations, *Planet. Space Sci.*, *24*, 79–85, doi:10.1016/0032-0633(76)90064-7.

Greenstadt, E. W., and J. V. Olson (1976), Pc 3, 4 activity and interplanetary field orientation, *J. Geophys. Res.*, *81*(34), 5911–5920, doi:10.1029/JA081i034p05911.

Greenstadt, E. W., M. M. Mellott, R. L. McPherron, C. T. Russell, H. J. Singer, and D. J. Knecht (1983), Transfer of pulsation-related wave activity across the magnetopause: Observations of corresponding spectra by ISEE-1 and ISEE-2, *Geophys. Res. Lett.*, *10*(8), 659–662, doi:10.1029/GL010i008p00659.

Hartinger, M., M. B. Moldwin, V. Angelopoulos, K. Takahashi, H. J. Singer, R. R. Anderson, Y. Nishimura, and J. R. Wygant (2010), Pc5 wave power in the quiet-time plasmasphere and trough: CRRES observations, *Geophys. Res. Lett.*, *37*, L07107, doi:10.1029/2010GL042475.

Heilig, B., H. Lühr, and M. Rother (2007), Comprehensive study of ULF upstream waves observed in the topside ionosphere by CHAMP and on the ground, *Ann. Geophys.*, *25*(3), 737–754, doi:10.5194/angeo-25-737-2007.

Heilig, B., P. R. Sutcliffe, D. C. Ndiitwani, and A. B. Collier (2013), Statistical study of geomagnetic field line resonances observed by CHAMP and on the ground, *J. Geophys. Res. Space Physics*, *118*, 1934–1947, doi:10.1002/jgra.50215.

Kepko, L., and H. E. Spence (2003), Observations of discrete, global magnetospheric oscillations directly driven by solar wind density variations, *J. Geophys. Res.*, *108*(A6), 1257, doi:10.1029/2002JA009676.

Kim, K. H., K. Takahashi, and B. J. Anderson (1998), Ground-satellite coherence analysis of Pc3 pulsations, *J. Geophys. Res.*, *103*, 11,755–11,769, doi:10.1029/98JA00617.

Kim, K. H., and K. Takahashi (1999), Statistical analysis of compressional Pc3–4 pulsations observed by AMPTE CCE at $L = 2–3$ in the dayside magnetosphere, *J. Geophys. Res.*, *104*, 4539–4558, doi:10.1029/1998JA900131.

Kim, K. H., K. Takahashi, D. H. Lee, P. Sutcliffe, and K. Yumoto (2005), Pi2 pulsations associated with poleward boundary intensifications during the absence of substorms, *J. Geophys. Res.*, *110*, A01217, doi:10.1029/2004JA010780.

Kivelson, M. G., J. Etcheto, and J. G. Trotignon (1984), Global compressional oscillations of the terrestrial magnetosphere—The evidence and a model, *J. Geophys. Res.*, *89*, 9851–9856, doi:10.1029/JA089iA11p09851.

Kletzing, C. A., et al. (2013), The Electric and Magnetic Field Instrument Suite and Integrated Science (EMFISIS) on RBSP, *Space Sci. Rev.*, *179*, 127–181, doi:10.1007/s11214-013-9993-6.

Koga, K., and T. Obara (2008), Development and measurement result of technical data acquisition equipment (TEDA) onboard ETS-VIII (in Japanese), *IEICE Tech. Rep.*, *108*(100), 23–25, Institute of Electronics, Information and Communication Engineers, Tokyo.

Kurth, W. S., S. D. Pascuale, J. B. Faden, C. A. Kletzing, G. B. Hospodarsky, S. Thaller, and J. R. Wygant (2015), Electron densities inferred from plasma wave spectra obtained by the Waves instrument on Van Allen Probes, *J. Geophys. Res. Space Physics*, *120*, 904–914, doi:10.1002/2014JA020857.

Kwon, H.-J., K.-H. Kim, C.-W. Jun, K. Takahashi, D.-H. Lee, E. Lee, H. Jin, J. Seon, Y.-D. Park, and J. Hwang (2013), Low-latitude Pi2 pulsations during intervals of quiet geomagnetic conditions ($Kp \leq 1$), *J. Geophys. Res. Space Physics*, *118*, 6145–6153, doi:10.1002/jgra.50582.

Lee, D. H. (1996), Dynamics of MHD wave propagation in the low-latitude magnetosphere, *J. Geophys. Res.*, *101*(A7), 15,371–15,386, doi:10.1029/96JA00608.

Lee, D. H., and R. L. Lysak (1999), MHD waves in a three-dimensional dipolar magnetic field: A search for Pi2 pulsations, *J. Geophys. Res.*, *104*(A12), 28,691–28,699, doi:10.1029/1999ja900377.

Lee, D.-H., and K. Takahashi (2006), MHD eigenmodes in the inner magnetosphere, in *Magnetospheric ULF Waves: Synthesis and New Directions, Geophys. Monogr. Ser.*, vol. 169, edited by K. Takahashi et al., pp. 73–90, AGU, Washington, D. C.

Love, J. J., C. A. Finn, K. L. Pedrie, and C. C. Blum (2015), The Boulder magnetic observatory, *U.S. Geol. Surv. Open-File Rep. 2015–1125*, U.S. Geol. Surv., Boulder, Colo., doi:10.3133/ofr20151125.

Luo, H., G. Chen, A. Du, V. Angelopoulos, W. Xu, X. Zhao, and Y. Wang (2011), THEMIS multipoint observations of Pi2 pulsations inside and outside the plasmasphere, *J. Geophys. Res.*, *116*, A12206, doi:10.1029/2011JA016746.

McFadden, J. P., C. W. Carlson, D. Larson, J. Bonnell, F. Mozer, V. Angelopoulos, K.-H. Glassmeier, and U. Auster (2008), THEMIS ESA first science results and performance issues, *Space Sci. Rev.*, *141*, 477–508, doi:10.1007/s11214-008-9433-1.

McKenzie, J. F. (1970), Hydromagnetic wave interaction with the magnetopause and the bow shock, *Planet. Space Sci.*, *18*(23), 1–23, doi:10.1016/0032-0633(70)90063-2.

McClay, J. F. (1970), On the resonant modes of a cavity and the dynamical properties of micropulsations, *Planet. Space Sci.*, *18*(12), 1673–1690, doi:10.1016/0032-0633(70)90002-4.

Moldwin, M. B., L. Downward, H. K. Rassoul, R. Amin, and R. R. Anderson (2002), A new model of the location of the plasmapause: CRRES results, *J. Geophys. Res.*, *107*(A11), 1339, doi:10.1029/2001JA009211.

Narita, Y., and K. H. Glassmeier (2005), Dispersion analysis of low-frequency waves through the terrestrial bow shock, *J. Geophys. Res.*, *110*, A12215, doi:10.1029/2005JA011256.

Nishida, A. (1978), *Geomagnetic Diagnosis of the Magnetosphere*, 256 pp., Springer, New York.

Nosé, M., K. Takahashi, T. Uozumi, K. Yumoto, Y. Miyoshi, A. Morioka, D. K. Milling, P. R. Sutcliffe, H. Matsumoto, and T. Goka (2003), Multipoint observations of a Pi2 pulsation on morning side: The September 20, 1995, event, *J. Geophys. Res.*, *108*(A5), 1219, doi:10.1029/2003JA009847.

Nosé, M., K. Takahashi, K. Keika, L. M. Kistler, K. Koga, H. Koshiishi, H. Matsumoto, M. Shoji, Y. Miyashita, and R. Nomura (2014), Magnetic fluctuations embedded in dipolarization inside geosynchronous orbit and their associated selective acceleration of O^+ ions, *J. Geophys. Res. Space Physics*, *119*, 4639–4655, doi:10.1002/2014JA019806.

Ponomarenko, P. V., C. L. Waters, and J.-P. St-Maurice (2010), Upstream Pc3–4 waves: Experimental evidence of propagation to the nightside plasmapause/plasmatrough, *Geophys. Res. Lett.*, *37*, L22102, doi:10.1029/2010GL045416.

Russell, C. T., P. J. Chi, D. J. Dearborn, Y. S. Ge, B. Kuo-Tiong, J. D. Means, D. R. Pierce, K. M. Rowe, and R. C. Snare (2008), THEMIS ground-based magnetometers, *Space Sci. Rev.*, *141*(1–4), 389–412, doi:10.1007/s11214-008-9337-0.

Samson, J. C., B. G. Harrold, J. M. Ruohoniemi, R. A. Greenwald, and A. D. M. Walker (1992), Field line resonance associated with MHD waveguides in the magnetosphere, *Geophys. Res. Lett.*, *19*, 441–444, doi:10.1029/92GL00116.

Shue, J.-H., et al. (1998), Magnetopause location under extreme solar wind conditions, *J. Geophys. Res.*, *103*(A8), 17,691–17,700, doi:10.1029/98JA01103.

Singer, H. J., L. Matheson, R. Grubb, A. Newman, and S. D. Bouwer (1996), Monitoring space weather with the GOES magnetometers, *Proc. SPIE Int. Soc. Opt. Eng.*, *2812*, 299–308.

Spreiter, J. R., A. L. Summers, and A. Y. Alksne (1966), Hydromagnetic flow around the magnetosphere, *Planet. Space Sci.*, *14*(3), 223–253, doi:10.1016/0032-0633(66)90124-3.

Sutcliffe, P. R., and K. Yumoto (1991), On the cavity mode nature of low-latitude Pi2 pulsations, *J. Geophys. Res.*, *96*(A2), 1543–1551, doi:10.1029/90JA02007.

Takahashi, K., R. L. McPherron, and T. Terasawa (1984), Dependence of the spectrum of Pc3–4 pulsations on the interplanetary magnetic field, *J. Geophys. Res.*, *89*, 2770–2780, doi:10.1029/JA089iA05p02770.

Takahashi, K., S. Ohtani, and K. Yumoto (1992), AMPTE CCE observations of Pi2 pulsations in the inner magnetosphere, *Geophys. Res. Lett.*, *19*, 1447–1450, doi:10.1029/92GL01283.

Takahashi, K., et al. (1994), GEOTAIL observation of magnetosonic Pc3 waves in the dayside magnetosphere, *Geophys. Res. Lett.*, *21*, 2899–2902, doi:10.1029/94GL01419.

Takahashi, K., D. H. Lee, M. Nosé, R. R. Anderson, and W. J. Hughes (2003a), CRRES electric field study of the radial mode structure of Pi2 pulsations, *J. Geophys. Res.*, *108*(A5), 1210, doi:10.1029/2002JA009761.

Takahashi, K., R. R. Anderson, and W. J. Hughes (2003b), Pi2 pulsations with second harmonic: CRRES observations in the plasmasphere, *J. Geophys. Res.*, *108*(A5), 1242, doi:10.1029/2002JA009747.

Takahashi, K., K. Liou, K. Yumoto, K. Kitamura, M. Nosé, and F. Honary (2005), Source of Pc4 pulsations observed on the nightside, *J. Geophys. Res.*, *110*, A12207, doi:10.1029/2005ja011093.

Takahashi, K., et al. (2010), Multipoint observation of fast mode waves trapped in the dayside plasmasphere, *J. Geophys. Res.*, *115*, A12247, doi:10.1029/2010JA015956.

Takahashi, K., R. E. Denton, W. Kurth, C. Kletzing, J. Wygant, J. Bonnell, L. Dai, K. Min, C. W. Smith, and R. MacDowall (2015a), Externally driven plasmaspheric ULF waves observed by the Van Allen Probes, *J. Geophys. Res. Space Physics*, *120*, 526–552, doi:10.1002/2014ja020373.

Takahashi, K., C. Waters, K.-H. Glassmeier, C. A. Kletzing, W. S. Kurth, and C. W. Smith (2015b), Multifrequency compressional magnetic field oscillations and their relation to multiharmonic toroidal mode standing Alfvén waves, *J. Geophys. Res. Space Physics*, *120*, 10,.384–10,403, doi:10.1002/2015ja021780.

Troitskaya, V. A. (1994), Discoveries of sources of Pc 2–4 waves—A review of research in the former USSR, in *Solar wind sources of magnetospheric ultra-low-frequency waves, Geophys. Monogr. Ser.*, vol. 81, edited by M. J. Engebreston, K. Takahashi, and M. Scholer, pp. 45–54, AGU, Washington, D. C.

Troitskaya, V. A., and O. V. Bolshakova (1988), Diagnostics of the magnetosphere using multipoint measurements of ULF waves, *Adv. Space Res.*, *8*(9–10), 413–425.

Troitskaya, V. A., T. A. Plyasova-Bakounina, and A. V. Gul'yel'mi (1971), Relationship between Pc2–4 pulsations and the interplanetary magnetic field, *Dokl. Akad. Nauk*, *197*, 1312.

Tsunomura, S., A. Yamazaki, T. Tokumoto, and Y. Yamada (1994), The new system of Kakioka automatic standard magnetometer, *Mem. Kakioka Mag. Obs.*, *25*(1–2), 3–32.

Tsyganenko, N. A. (1989), A magnetospheric magnetic field model with a warped tail current sheet, *Planet. Space Sci.*, *37*, 5–20, doi:10.1016/0032-0633(89)90066-4.

Vellante, M., U. Villante, M. De Lauretis, and G. Barchi (1996), Solar cycle variation of the dominant frequencies of Pc3 geomagnetic pulsations at $L = 1.6$, *Geophys. Res. Lett.*, *23*(12), 1505–1508.

Wolfe, A., and R. L. Kaufmann (1975), MHD wave transmission and production near the magnetopause, *J. Geophys. Res.*, *80*(13), 1764–1775, doi:10.1029/JA080i013p01764.

Wright, A. N. (1994), Dispersion and wave coupling in inhomogeneous MHD waveguides, *J. Geophys. Res.*, *99*(A1), 159–167, doi:10.1029/93JA02206.

Wygant, J. R., et al. (2013), The electric field and waves instruments on the radiation belt storm probes mission, *Space Sci. Rev.*, *179*, 183–220, doi:10.1007/s11214-013-0013-7.

Yeoman, T. K., and D. Orr (1989), Phase and spectral power of mid-latitude Pi2 pulsations: Evidence for a plasmaspheric cavity resonance, *Planet. Space Sci.*, *37*(11), 1367–1383, doi:10.1016/0032-0633(89)90107-4.
Yumoto, K., and T. Saito (1983), Relation of compressional HM waves at GOES 2 to low-latitude Pc3 magnetic pulsations, *J. Geophys. Res.*, *88*(A12), 10,041–10,052, doi:10.1029/JA088iA12p10041.
Yumoto, K., and The 210° MM Magnetic Observation Group (1996), The STEP 210° magnetic meridian network project, *J. Geomagn. Geoelectr.*, *48*, 1297–1309.
Yumoto, K., T. Saito, S.-I. Akasofu, B. T. Tsurutani, and E. J. Smith (1985), Propagation mechanism of daytime Pc3–4 pulsations observed at synchronous orbit and multiple ground-based stations, *J. Geophys. Res.*, *90*(A7), 6439, doi:10.1029/JA090iA07p06439.